Raman studies of amorphous nanocarbon obtained by laser sputtering

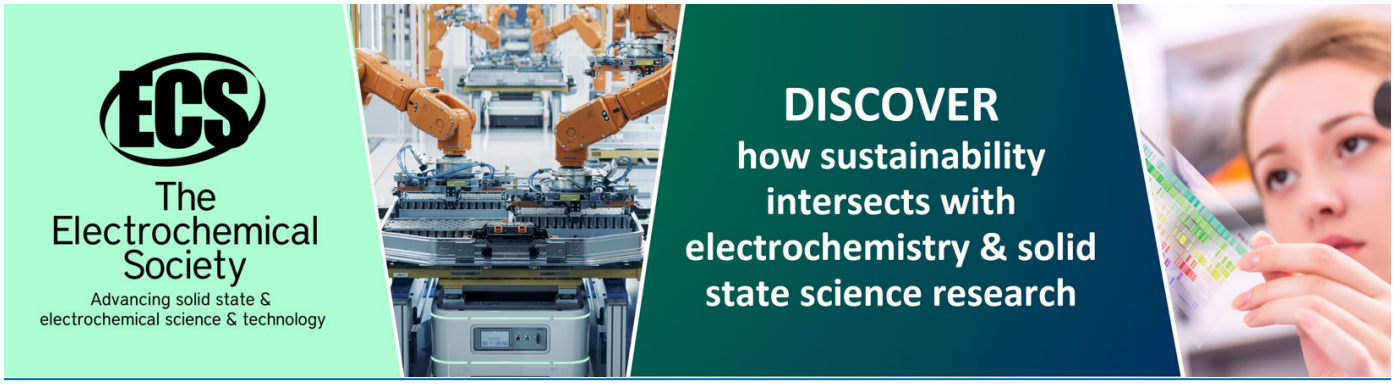

Raman studies of amorphous nanocarbon obtained by laser sputtering

I A Eliseyev[1], A N Smirnov[1,*], V Yu Davydov[1], A V Platonov[1], D A Yavsin[1] and S A Gurevich[1]

[1]Ioffe Institute, St. Petersburg, 194021, Russia

*Corresponding author e-mail: alex.smirnov@mail.ioffe.ru

Abstract. The structural properties of amorphous nanocarbon films fabricated by laser sputtering of a graphite target are investigated by means of Raman spectroscopy. Analysis of the spectral features in the region of 100–3600 cm^{-1} allowed us to determine the allotrope composition of the films and the degree of disorder in terms of average crystallite size. The results obtained are important for application of such films in the field of electrode coatings.

1. Introduction

Carbon materials, due to a significant variety of their physical and chemical properties, are used in various fields, from metallurgy, structural materials, absorbents and filters, to use in catalysis [1], or, for example, as additives that modify the properties of plastics [2]. Recently, use of carbon structures in electric energy storage devices - lithium-ion batteries [3] – has become one of the most important areas of application of such structures. In this area, one of the directions is the use of fine powders of amorphous carbon or carbon fibers with high conductivity as additives to cathode materials, usually poorly conductive, to ensure the required level of electrical conductivity of electrode layers [4]. In another version, various carbon micro- and nanostructured materials are used as anode materials for lithium-ion batteries, as an alternative to traditional graphite powders [5]. In this case, the main task is to ensure the maximum value of the specific capacity of the anode material in relation to the accumulation of lithium atoms. Recently, we have found that coatings of amorphous nanocarbon obtained by laser sputtering of a graphite target have an extremely high specific capacity for lithium [6]. In this work, preliminary results of studying the properties of the resulting structures were also presented. The purpose of this work is to study in more detail the structural properties of amorphous nanocarbon obtained by laser evaporation, with the main emphasis on studies by the method of Raman spectroscopy.

2. Experimental

Films of amorphous nanocarbon, from a few to tens of microns thick, were obtained by sputtering an isostatic graphite target with a Nd:YAG laser with a wavelength of 1.06 μm, a pulse duration of 25 ns, and a pulse energy of 200 mJ. The radiation was focused on the target surface into a spot about 1 mm in diameter, with the specific radiation power on the target surface being about 10^{13} W/m^2. The process was carried out in a vacuum chamber at a pressure of 10^{-4} Pa.

Raman spectra were obtained using a Horiba Jobin-Yvon T64000 spectrometer. The use of confocal optics and an objective with a magnification of 100×, a numerical aperture of 0.9 and an increased focal length (1 mm) made it possible to obtain information from a sample region with a

diameter of ~ 1 mm. The spectra of each of the samples were recorded at several points, and averaged spectra were used to analyze the structural characteristics. To excite the Raman spectra, a Nd:YAG laser with a wavelength of 532 nm was used. To exclude the heating and damage of the samples due to the laser radiation, the laser power during measurements was limited to 1 mW.

3. Raman spectroscopy of disordered carbon

For characterization of the films, the method of Raman spectroscopy was used. This technique is standard for studying all types of carbon structures: from single-crystal graphite to diamond-like nanocrystalline films [7]. When studying nanocarbon films, it allows one to determine the average crystallite size [8–11], the fraction of sp^3 carbon [12–14], the presence of sp^1 carbon chains [15, 16], the content of impurities [12, 17, 18], and many other structural factors by analyzing the parameters of individual lines of the Raman spectrum.

Determination of the main type of hybridization and the average crystallite size, which are the key parameters for the films under study, is based on the "amorphization trajectory" approach, first introduced in [7]. This approach allows one to distinguish the type of structure of the material under study (nanocrystalline graphite, sp^2 or sp^3 amorphous carbon) by analyzing the parameters of the *D* and *G* lines in the Raman spectra. In particular, the position of the *G* line and the intensity ratio of the *D* and *G* lines ($I(D)/I(G)$) are used for the analysis. The amorphization trajectory goes from monocrystalline graphite to tetragonal amorphous carbon, and includes three stages (graphite-nanographite transition – stage 1, nanographite - amorphous sp^2 carbon transition – stage 2, and stage 3 – amorphous sp^2 carbon - amorphous sp^3 carbon transition). It should be noted that stage 2 is fundamentally different from stage 1 by the presence of topological disorder: while in stage 1 the crystallites still have a predominantly hexagonal crystal lattice, then in stage 2 pentagonal and heptagonal carbon rings, as well as a large number of dangling bonds, appear in the lattice [12]. With the transition from one stage to another, the character of the dependence of the line intensity ratio on the crystallite size changes.

The Raman spectra of nanocarbon films studied in this work were recorded in the region of 100–3200 cm^{-1}. Spectrum of graphite in this range contains of two main lines: the *G* line (~1580 cm^{-1}), and the 2*D* line (~2700 cm^{-1}). The *G* line is associated with vibrations along the sp^2 C=C bond and corresponds to the vibrational mode E_{2g} in the crystal lattice of graphite; therefore, it is characteristic of any carbon compounds with sp^2 bonds. In case of amorphous carbons, the frequency of the *G* line depends on the degree of amorphization: it experiences a blueshift from 1580 to 1600 cm^{-1} with increasing amorphization on stage 1, then the frequency gradually falls to ~1510 cm^{-1} during stage 2 and rises again to 1570 cm^{-1} at the end of stage 3 due to the transition of the majority of the sp^2 rings to olefinic groups, in which the bonds have slightly higher vibrational frequencies [7].

The *D* line is related to the iTO (in-plane TO) phonon at the K point of the Brillouin zone, which corresponds to fully symmetric "breathing" vibrations of hexagonal carbon rings. In the Raman spectra of an ideal crystal, the appearance of lines corresponding to phonons with a nonzero wave vector is prohibited by the selection rules. Violation of the selection rules can occur with the participation of crystal lattice defects in the scattering process, or in case of so-called double-resonance Raman scattering [19]. Thus, the *D* line can appear in the presence of defects in the crystal lattice of hexagonal carbon, and its intensity reflects the number of defects. It is important to note that, within the framework of the amorphization trajectory approach, the intensity of the *D* line associated with breathing vibrations of hexagonal carbon rings will increase with increasing defect concentration only at the first stage of amorphization, when the crystal structure of the sample is predominantly formed by hexagonal rings. With the appearance of dangling bonds, non-hexagonal rings and chains in the crystal lattice, the intensity of the *D* line begins to decrease, and new lines appear in the spectra. In this case, the spectrum in the range of 1000–1700 cm^{-1} is no longer described only with 2 Lorentzian *G* and *D* peaks, but has a complex structure with up to 6 components [20]. Component *D3* corresponds to the amorphous sp^2 carbon fraction in soot and carbon black, and its intensity reflects the fraction of amorphous carbon in the crystal lattice [20]. Component *D4* (~1100–1200 cm^{-1}) corresponds to the

peak of the density of vibrational states in the phonon dispersion of graphite [21]. In some works, its appearance is associated with the presence of topological disorder in the graphite lattice: sp^3 bonds [12], inclusions of hexagonal diamond (lonsdaleite) [22], as well as non-hexagonal carbon rings and carbon chains [15] and mixed sp^2–sp^3 bonds [23].

4. Results and discussion

Figure 1a shows the spectra obtained from seven different nanocarbon films prepared by laser evaporation. The spectra for different samples have minor differences in their shape. Figure 2 shows the simulation of experimental spectra in the range 1000–1700 cm^{-1} using four components: *G* (~ 1580 cm^{-1}), *D* (~ 1350 cm^{-1}), *D3* (~ 1500 cm^{-1}) and *D4* (~ 1200 cm^{-1}) [24].

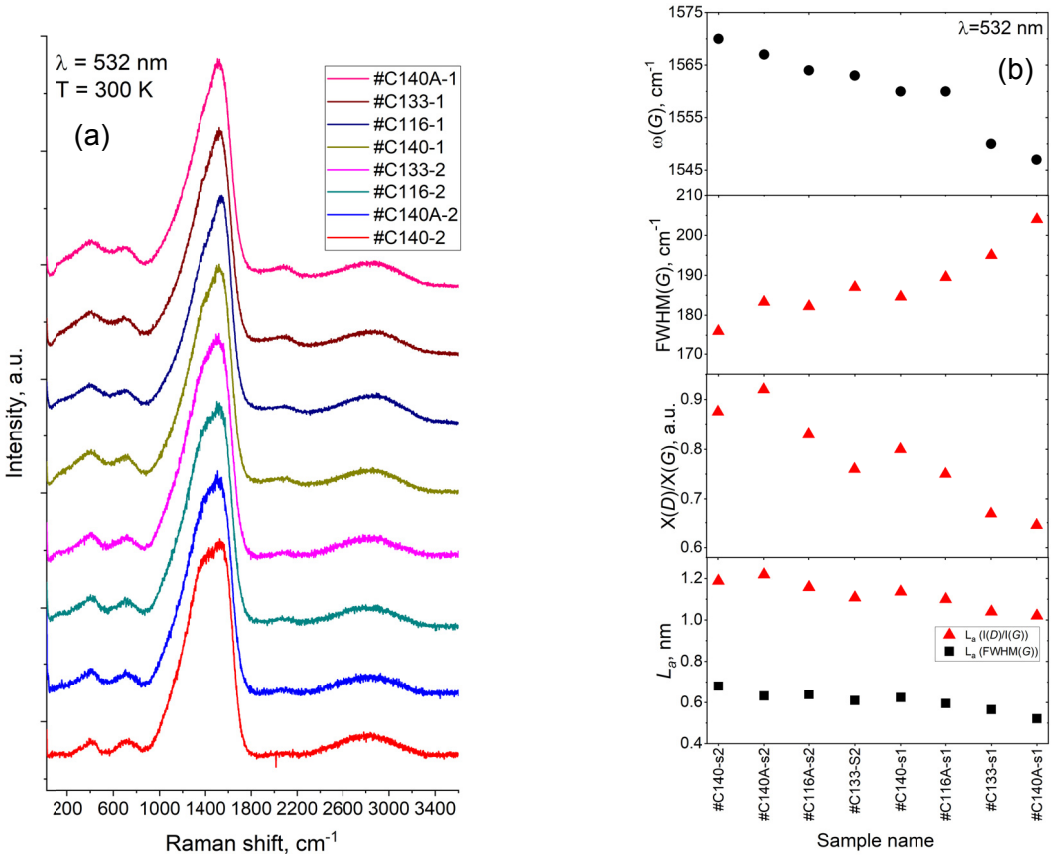

Figure 1. (a) Raman spectra of the seven studied nanocarbon samples. The spectra are presented in ascending order of the degree of amorphization (according to the average crystallite size). (b) Frequency and *FWHM* of the *G* line (ω_G), peak intensity ratios of the *D* and *G* lines ($I(D)/I(G)$), and the average crystallite size (L_a) estimates for every studied sample.

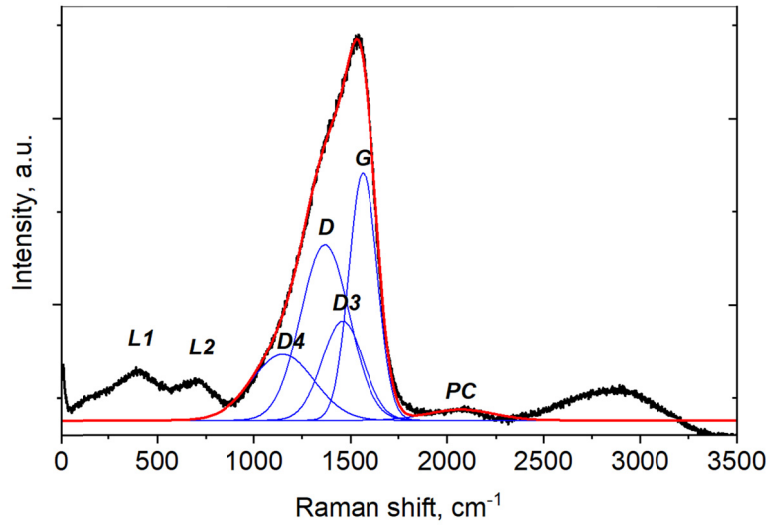

Figure 2. An example of modelling of the spectra. Black line represents the experimental data, blue lines show the fitted components, and the red line is the sum of the fitted components.

The spectra of all samples presented in this work contain the contribution of the *D3* and *D4* lines, which indicates the presence of topological disorder. Position of the *G* line ranges from 1545 to 1570 cm^{-1}. This frequency range may either correspond to the second or to the third stage of amorphization. However, in the third amorpization stage, due to the absence of sixfold rings, the *D* line must be almost absent ($I(D)/I(G)<0.1$), which is wrong in our case. In the region of higher frequencies, an almost symmetric wide band ranging from 2400 to 3100 cm^{-1} is visible, which is characteristic of second amorphization stage [7]. Thus, the samples under study should be attributed to the second stage of amorphization. At this stage, we can estimate the average crystallite size using the formula from [7]:

$$L_a(\text{nm}) = 0.1\sqrt{\frac{I(D)}{I(G)C'(\lambda)}} \quad (1)$$

where C' for the used wavelength of 532 nm = 0.0062 [7, 25], L_a is the average crystallite size, $I(D)$ and $I(G)$ are the peak intensities of the *D* and *G* lines, respectively. In addition to the line intensity ratio, the full width at half maximum of the *G* line ($FWHM(G)$) is also used to estimate the crystallite size. In this case, the formula for obtaining the crystallite size is as follows [11]:

$$L_a(\text{nm}) = \left(\frac{142.1}{FWHM(G)}\right)^{1.802} \quad (2)$$

Figure 1b shows data on various parameters of the spectral lines of the studied carbon samples, as well as the average crystallite size calculated using formulae (1) and (2). In this case, the samples themselves are arranged in the order of increasing degree of amorphization, that is, decreasing the average crystallite size.

In addition to the *G*, *D*, *D3*, and *D4* lines, other features are observed in the spectra. Two broad peaks *L1* and *L2* at low frequencies correspond to the maxima of the density of vibrational states of graphite [26]. The manifestation of the density of vibrational states with an intensity comparable to the intensity of the main lines of the Raman spectra indicates extremely small cluster sizes: in the case of silicon, such features could be detected in the spectra at a cluster size of 1 nm [27], while for carbon, these features were manifested in the spectra of samples with the sizes of carbon clusters 1–3 nm [26]. It was shown in [17] that these features are characteristic of pure amorphous carbon and are absent in the spectra of amorphous hydrogenated carbon (*a*-C:H). Thus, it can be assumed that all studied samples are free of hydrogen impurities. An additional confirmation of this assumption is the absence in the spectra of a photoluminescence background that grows with an increase in the wavenumber associated with hydrogen passivation of nonradiative recombination centers [18].

Another feature of the spectra of the studied samples is a wide asymmetric profile in the range of 1750–2250 cm^{-1} (denoted as *PC* in figure 2). Its low-frequency wing (1800–1870 cm^{-1}) corresponds to

cumulene carbon sp^1 chains with a predominance of carbon-carbon double bonds (C=C), and the high-frequency part (1980–2100 cm^{-1}) corresponds to polyyne sp^1 chains with alternating triple and single C–C bonds [15, 16]. When considering the spectra in figure 1a, it can be seen that the intensity of the *PC* band decreases with an increase in the degree of amorphization. This indicates that the fraction of sp^1 chains in the samples is inversely proportional to the average crystallite size.

Analyzing the form of the spectra shown in figure 1a, it can be assumed that the studied samples are quite close to each other in their structural characteristics. Nevertheless, the analysis of the parameters of the spectral lines shows significant differences in the estimates of the crystallite sizes for the studied samples. In the presence of various methods for assessing the size of crystallites, the question arises as to the choice between them. An estimate using the ratio of the intensities of spectral lines can give ambiguous results for several reasons. First, there is still no consensus in the literature on which kind of line intensity - peak or integral - should be used for estimation. Second, as mentioned above, the dependence of the intensity of the *D* line on the crystallite size behaves differently depending on the stage of amorphization. As a consequence, the same value of the $I(D)/I(G)$ ratio can give radically different estimates depending on the stage of amorphization to which the sample is assigned. The broadening mechanism of the *G* line is based on the localization of phonons in crystallites and is related to their size much more unambiguously than the $I(D)/I(G)$ ratio. Thus, the estimates of the crystallite size based on the $FWHM(G)$ analysis should be more correct. In our case, the estimates obtained using expression (1) from the ratio of the intensities of the spectral lines are twice as high as the estimates obtained using expression (2). Nevertheless, in order of magnitude, the particle size obtained using both expressions is in agreement with the characteristic particle sizes (1–3 nm) of the samples studied in [26], in the spectra of which, as in our case, two broad bands were observed in the 300–900 cm^{-1} frequency region.

5. Conclusion

Raman spectroscopy was used to determine the composition of amorphous nanocarbon films prepared by laser sputtering. It was found that the studied samples are predominantly composed of graphitic carbon with the presence of a significant fraction of inclusions of amorphous carbon, sp^3-phase, as well as polyyne and cumulene chains. In addition, it was shown that the studied samples do not contain hydrogen. Using the parameters of spectral lines obtained by approximation of experimental data, the sizes of crystallites in the studied samples were estimated.

Acknowledgments

This research was supported within the State Assignments from the Ministry of Science and Higher Education of the Russian Federation to the Ioffe Institute (0040-2019-0006).

References

[1] Ahmed A I, Mandal S, Gines L, Williams O A and Cheng C L 2016 Low temperature catalytic reactivity of nanodiamond in molecular hydrogen *Carbon N. Y.* **110** 438–42
[2] Spahr M E and Rothon R 2017 Carbon Black as a Polymer Filler pp 261–91
[3] Zhang H, Zhao H, Khan M A, Zou W, Xu J, Zhang L and Zhang J 2018 Recent progress in advanced electrode materials, separators and electrolytes for lithium batteries *J. Mater. Chem. A* **6** 20564–620
[4] Cho I, Choi J, Kim K, Ryou M H and Lee Y M 2015 A comparative investigation of carbon black (Super-P) and vapor-grown carbon fibers (VGCFs) as conductive additives for lithium-ion battery cathodes *RSC Adv.* **5** 95073–8
[5] Guo Z, Wang C, Chen M and Li M 2013 Hard carbon derived from coal tar pitch for use as the anode material in lithium ion batteries *Int. J. Electrochem. Sci.* **8** 2702–9
[6] Gurevich S A, Gorokhov M V., Kozhevin V M, Kukushkin M V., Levitskii V S, Markov L K and Yavsin D A 2018 Formation of Amorphous Carbon Nanoparticles by the Laser Electrodispersion Method *Tech. Phys. Lett.* **44** 207–9

[7] Ferrari A C and Robertson J 2000 Interpretation of Raman spectra of disordered and amorphous carbon *Phys. Rev. B* **61** 14095–107
[8] Tuinstra F and Koenig J L 1970 Raman Spectrum of Graphite *J. Chem. Phys.* **53** 1126–30
[9] Caṇado L G, Takai K, Enoki T, Endo M, Kim Y A, Mizusaki H, Jorio A, Coelho L N, Magalhães-Paniago R and Pimenta M A 2006 General equation for the determination of the crystallite size la of nanographite by Raman spectroscopy *Appl. Phys. Lett.* **88** 1–4
[10] Puech P, Kandara M, Paredes G *et al* 2019 Analyzing the Raman Spectra of Graphenic Carbon Materials from Kerogens to Nanotubes : What Type of Information Can Be Extracted from Defect Bands *C - J. Carbon Res.* **5** 69
[11] Ferrari A C, Rodil S E, Robertson J, Rodil S E and Robertson J 2003 Interpretation of infrared and Raman spectra of amorphous carbon nitrides *Phys. Rev. B* **67** 155306
[12] Ferrari A C and Robertson J 2004 Raman spectroscopy of amorphous, nanostructured, diamond–like carbon, and nanodiamond *Philos. Trans. R. Soc. London. Ser. A Math. Phys. Eng. Sci.* **362** 2477–512
[13] Prawer S, Nugent K W, Lifshitz Y, Lempert G D, Grossman E, Kulik J, Avigal I and Kalish R 1996 Systematic variation of the Raman spectra of DLC films as a function of sp^2 :sp^3 composition *Diam. Relat. Mater.* **5** 433–8
[14] Zhang S, Zeng X T, Xie H and Hing P 2000 A phenomenological approach for the ID/IG ratio and sp^3 fraction of magnetron sputtered a-C films *Surf. Coatings Technol.* **123** 256–60
[15] Le K C, Lefumeux C, Bengtsson P E and Pino T 2019 Direct observation of aliphatic structures in soot particles produced in low-pressure premixed ethylene flames via online Raman spectroscopy *Proc. Combust. Inst.* **37** 869–76
[16] Ravagnan L, Siviero F, Lenardi C, Piseri P, Barborini E, Milani P, Casari C S, Li Bassi A and Bottani C E 2002 Cluster-Beam Deposition and in situ Characterization of Carbyne-Rich Carbon Films *Phys. Rev. Lett.* **89** 285506
[17] Tamor M A and Vassell W C 1994 Raman '"fingerprinting"' of amorphous carbon films *J. Appl. Phys.* **76** 3823–30
[18] Casiraghi C, Ferrari A C and Robertson J 2005 Raman spectroscopy of hydrogenated amorphous carbons *Phys. Rev. B* **72** 085401
[19] Ferrari A C and Basko D M 2013 Raman spectroscopy as a versatile tool for studying the properties of graphene. *Nat. Nanotechnol.* **8** 235–46
[20] Pawlyta M, Rouzaud J N and Duber S 2015 Raman microspectroscopy characterization of carbon blacks: Spectral analysis and structural information *Carbon* **84** 479–90
[21] Couzi M, Bruneel J L, Talaga D and Bokobza L 2016 A multi wavelength Raman scattering study of defective graphitic carbon materials: The first order Raman spectra revisited *Carbon N. Y.* **107** 388–94
[22] Silva S R P, Amaratunga G A J, Salje E K H and Knowles K M 1994 Evidence of hexagonal diamond in plasma-deposited carbon films *J. Mater. Sci.* **29** 4962–6
[23] Dippel B, Jander H and Heintzenberg J 1999 NIR FT Raman spectroscopic study of flame soot *Phys. Chem. Chem. Phys.* **1** 4707–12
[24] Sadezky A, Muckenhuber H, Grothe H, Niessner R and Pöschl U 2005 Raman microspectroscopy of soot and related carbonaceous materials: Spectral analysis and structural information *Carbon* **43** 1731–42
[25] Matthews M J, Pimenta M A, Dresselhaus G, Dresselhaus M S and Endo M 1999 Origin of dispersive effects of the Raman D band in carbon materials *Phys. Rev. B - Condens. Matter Mater. Phys.* **59** 6585–8
[26] Li F and Lannin J S 1992 Disorder induced Raman scattering of nanocrystalline carbon *Appl. Phys. Lett.* **61** 2116–8
[27] Alben R, Weaire D, Smith J E and Brodsky M H 1975 Vibrational properties of amorphous Si and Ge *Phys. Rev. B* **11** 2271–96